Catalysis Communications 60 (2015) 129–133

Contents lists available at ScienceDirect

Catalysis Communications

journal homepage: www.elsevier.com/locate/catcom

Short communication

TiO_2/SnO_2 double-shelled hollow spheres-highly efficient photocatalyst for the degradation of rhodamine B

Jujun Yuan [a,*], Xianke Zhang [a], Hongdong Li [b], Kai Wang [b], Shiyong Gao [c,*], Zhen Yin [a], Huajun Yu [a], Xiurong Zhu [a], Zuzhou Xiong [a], Yingmao Xie [a]

[a] *School of Physics and Electronics, Gannan Normal University, Ganzhou 341000, PR China*
[b] *State Key Laboratory of Superhard Materials, Jilin University, Changchun 130012, PR China*
[c] *School of Materials Science and Engineering, Harbin Institute of Technology, Harbin 150001, PR China*

ARTICLE INFO

Article history:
Received 20 October 2014
Received in revised form 28 November 2014
Accepted 29 November 2014
Available online 2 December 2014

Keywords:
Hollow spheres
Liquid-phase deposition
Photocatalysis
SnO_2
TiO_2

ABSTRACT

TiO_2/SnO_2 double-shelled hollow spheres are successfully synthesized by two-step liquid-phase deposition method using carbon sphere templates. The formation process of TiO_2/SnO_2 hollow spheres is discussed. The samples are characterized by X-ray diffraction, scanning electron microscopy, transmission electron microscopy, high-resolution transmission electron microscopy and UV–vis absorption spectroscopy. The behavior of photogenerated charges in the TiO_2/SnO_2 heterojunction structures has been investigated through surface photovoltage spectroscopy. The TiO_2/SnO_2 hollow spheres which are realized show significantly enhanced photocatalytic activities, with respect to the cases of SnO_2 and TiO_2 hollow spheres. Furthermore, TiO_2/SnO_2 hollow spheres show good recyclable photocatalytic activities.

1. Introduction

Environmental problems, such as organic pollutants and toxic water pollutants, provide the impetus for fundamental and applied research in the environmental area. Semiconductor photocatalysts exhibit several properties that are strongly sensitive to their structures, and are considered to be important materials for environmental applications [1–4]. However, the relatively low quantum yield that is normally caused due to rapid recombination of photogenerated electrons and holes hinders the commercialization of this technology [5]. In order to enhance the quantum yield, the application of heterojunction oxide structures, such as ZnO/SnO_2 [6,7], TiO_2/SnO_2 [8,9], and WO_3/TiO_2 [10,11], have been further introduced because the heterojunction could provide a potential driving force (the internal electrostatic potential in the space charge region) to reduce the recombination of photogenerated charge carriers.

Among these semiconductor oxides, TiO_2 and SnO_2, well-known wide direct band gap n-type semiconductors, are considered as the most promising functional materials due to their unique physical and chemical properties [12,13]. In the past decade, more and more TiO_2/SnO_2 nanomaterials have been reported to improve photocatalytic efficiency, because these nanomaterials possess heterojunction structure and a high surface area, which can provide both effective driving force and convenient way for photogenerated carriers to transfer to the reaction surfaces. For example, TiO_2/SnO_2 composite nanoparticles had been fabricated by one-step flame to get improved photocatalytic activity [14]. Efficient bicomponent TiO_2/SnO_2 nanofiber photocatalysts were prepared by electrospinning method [15,16]. Sieve-like SnO_2/TiO_2 nanotubes also showed enhanced photocatalytic efficiency, which had been fabricated by assembling sieve-like macroporous Sb-doped SnO_2 film on vertically aligned TiO_2 nanotubes through a block copolymer soft-template method [17]. However, there are few studies on TiO_2/SnO_2 hollow spheres as efficient and low-cost photocatalysts.

In this paper, we report the SnO_2/TiO_2 double-shelled hollow spheres synthesized by a two-step liquid-phase deposition (LPD) method using carbon spheres as the templates for the first time. The SnO_2/TiO_2 hollow spheres, which have been achieved, show highly efficient photocatalytic activities for the decomposition of rhodamine B (RhB).

2. Experimental

2.1. Fabrication of SnO_2/TiO_2 hollow spheres

Carbon spheres were prepared by the hydrothermal method according to a reported procedure [18]. In a typical procedure, 4 g of glucose was dissolved in 30 mL of deionized water, and then the resulting solution was transferred to a 50 mL Teflon-lined autoclave and maintained at 180 °C for 20 h. The products were centrifuged and rinsed for several times with distilled water and finally dried at 80 °C for 12 h. For the

---

* Corresponding authors.
E-mail addresses: yuanjvjun@aliyun.com (J. Yuan), gaoshiyong@hit.edu.cn (S. Gao).

http://dx.doi.org/10.1016/j.catcom.2014.11.032
1566-7367/

preparation of SnO_2 shell, 0.3 g of carbon spheres was dispersed and immersed in the aqueous solution of SnF_2 (0.02 M) under stirring at 50 °C for 8 h. The products were centrifuged and dried at 80 °C for 12 h. For the fabrication of TiO_2 shell, carbon spheres with SnO_2 shell are dispersed and immersed in the aqueous solution of ammonium hexafluorotitanate (0.05 M) and boric acid (0.15 M) under stirring at 50 °C for 40 min. The resulting products were dried at 80 °C for 12 h, followed by calcination at 550 °C for 4 h in air. TiO_2/SnO_2 double-shelled hollow spheres were finally obtained. For comparison, SnO_2 and TiO_2 hollow spheres are also fabricated with the same process to obtain the SnO_2 shell and TiO_2 shell, respectively.

2.2. Characterization

The structure and morphologies of the samples were characterized by means of X-ray diffraction (XRD), scanning electron microscopy (SEM), transmission electron microscopy (TEM) and high-resolution transmission electron microscopy (HRTEM). The element signatures of the samples were characterized by energy-dispersive X-ray (EDX). The UV–vis transmission optical properties were texted by UV-3150 double-beam. The specific surface area was determined by using the standard Brunauer–Emmett–Teller (BET) method. The separation characteristics of photogenerated charge carriers were tested by a lock-in-based surface photovoltage (SPV) measurement system.

2.3. Photocatalytic evaluation

The photocatalytic activities of TiO_2/SnO_2 hollow spheres were investigated by measuring the photodegradation rate of RhB aqueous solution. The reaction suspension was prepared by adding the sample (10 mg) into a 10 mL of RhB (10 mg L^{-1}) solution. The suspension was stirred in the dark for 1 h to ensure an adsorption/desorption equilibrium prior to UV irradiation. The suspension was then irradiated by an Hg lamp (500 W) under continuous stirring. The remaining amounts of RhB in solution were determined by measuring the absorption intensity of the main peak at 554 nm by UV–vis spectrophotometer (KD723PC).

3. Result and discussion

The crystallinity of composite hollow spheres was examined by powder XRD measurements (Fig. S1). It can be seen that there are two sets of diffraction peaks. One set of diffraction peaks is indexed to the rutile SnO_2 phases (JCPDS file.03-1114). The other set of peaks is connected to the anatase TiO_2 phases (JCPDS file.02-387). No characteristic peaks for impurity were observed, which further confirmed the composition of SnO_2 and TiO_2 in the heterostructure.

Fig. 1a shows the typical SEM image of carbon spheres. The average diameter is about 460–520 nm. From Fig. 1b, it can be seen that the

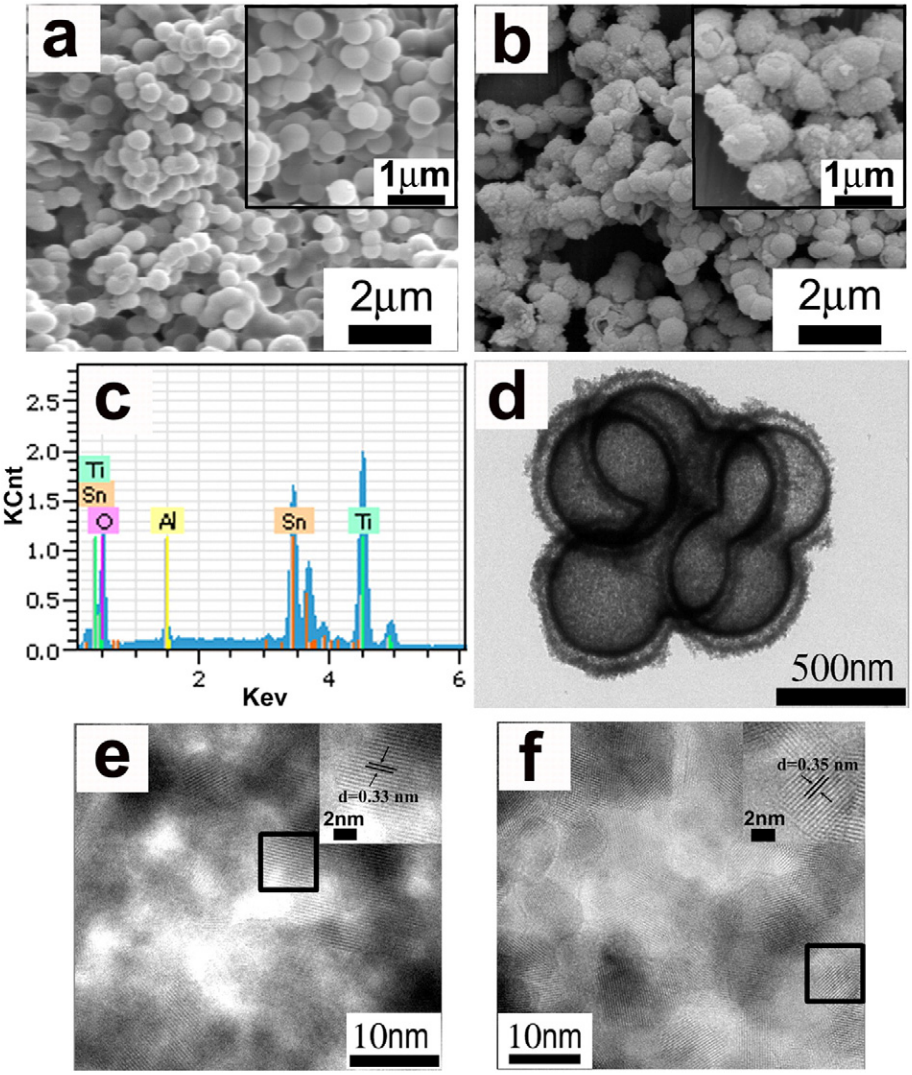

Fig. 1. Low and high (inset) magnifications of SEM images of carbon sphere templates (a) and TiO_2/SnO_2 hollow spheres (b). (c) EDX spectrum of TiO_2/SnO_2 hollow spheres. (d) TEM images of TiO_2/SnO_2 hollow spheres. HRTEM image of SnO_2 shell (e) and TiO_2 shell (f).

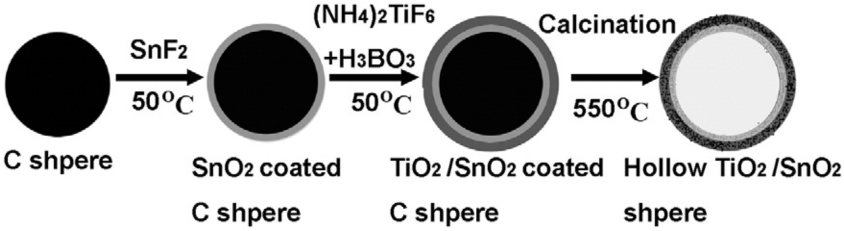

Fig. 2. Schematic of the steps for forming the TiO_2/SnO_2 hollow spheres.

hollow spheres have average diameters of ~550–700 nm and some spheres show open features with two shells, indicating that TiO_2/SnO_2 hollow spheres have been fabricated successfully. Fig. 1c shows the chemical analysis of the TiO_2/SnO_2 hollow spheres by EDX analysis. From the EDX result, it can be observed that the dominant elements in the hollow spheres are stannum, titanium, and oxygen. A more detailed view of the morphology and microstructure of hollow spheres has been obtained by means of TEM. TEM images of the spheres clearly depict the remarkable contrast between the peripheral and internal parts (Fig. 1d). It is evident the hollow spheres are formed with two shells. Close examination shows that the inner shell (SnO_2) has a thickness of ~30–35 nm and outer shell (TiO_2) has a thickness of ~60–70 nm. Fig. 1e and f shows HRTEM images of SnO_2 and TiO_2 shells respectively. The clear and aligned lattice fringes, with a mean interplanar spacing of about 0.33 nm (Fig. 1e), correspond to the (110) plane of tetragonal SnO_2. The distance between the adjacent lattice fringes corresponds to the interplanar distance of the tetragonal TiO_2 (101), which is d (101) = 0.35 nm (Fig. 1f).

The N_2 adsorption–desorption isotherms of the calcined TiO_2/SnO_2 hollow spheres at liquid nitrogen temperature (77 K) have been plotted in Fig. S2. The isotherm exhibits a type IV with type H4 hysteresis loop, which is characteristic of mesoporous solid materials [19,20]. As revealed from the Barrett–Joyner–Halenda (BJH) pore size distribution (the inset of Fig. S2), the average mesopore size is about 3.5 nm and pore volume is about 0.2 cm^3/g. The BJH analysis indicates that the overall BET surface area of TiO_2/SnO_2 hollow spheres is 46.1 m^2/g.

The above results show that we have successfully prepared TiO_2/SnO_2 hollow spheres using a simple two-step LPD approach. Fig. 2 illustrates schematically the steps for the formation of the hollow spheres. The process starts with growing carbon spheres by a hydrothermal method. This is followed by the deposition of SnO_2 on the carbon spheres. The reaction is summarized as the following [21]:

$$SnF_2 + H_2O + 1/2O_2 \leftrightarrow SnO_2 + 2H^+ + 2F^-. \tag{1}$$

In the first step of synthesis system, the SnO_2 is formed on the carbon spheres by a hydrolysis of SnF_2. For the formation of TiO_2 shell, the reactions are described as the following [22,23]:

$$TiF_6{}^{2-} + 2H_2O \leftrightarrow TiO_2 + 4HF + 2F^- \tag{2}$$

$$H_3BO_3 + 4HF \leftrightarrow BF_4{}^- + 3H_2O + H^+. \tag{3}$$

In the synthesis system, the TiO_2 is formed by hydrolysis of Ti-fluoro complex ions as in Eq. (2). As shown in Eq. (3), the added boric acid acts as a scavenger for F^-. Lastly, the TiO_2/SnO_2 hollow spheres can be obtained by wiping off carbon spheres during the process of calcination.

The UV–visible absorption spectrum of TiO_2/SnO_2 hollow spheres is shown in Fig. 3a. For comparison, the absorption spectrum of SnO_2 and TiO_2 hollow spheres are also presented. In the direct transition semiconductor, the optical absorption coefficient (α) and the band gap energy (E_g) are related by $\alpha h\nu = D(h\nu - E_g)^{1/2}$, where h is the Planck's constant, ν is the frequency of the incident photon, E_g is the optical band gap and D is constant. The variations of $(\alpha h\nu)^2$ versus the photon energy $h\nu$ in the fundamental absorption region are plotted in the inset of Fig. 3a. The E_g values of the SnO_2, TiO_2 and TiO_2/SnO_2 hollow spheres are 3.59, 3.36 and 3.45 eV, respectively, by extrapolating the linear portion to the photon energy axis. This experimental result shows that the presence of TiO_2 in the TiO_2/SnO_2 hollow spheres contributed to a red shift of the absorption edge compared with the SnO_2 hollow spheres. It is evident that the formation of TiO_2/SnO_2 heterojunctions modified the electronic structures of the pristine semiconductors.

The results of surface photovoltage spectroscopy (SPS) of the samples are shown in Fig. 3b. SPS presents the SPV amplitude as a function of the incident wavelength. SPS is a well-established contactless and nondestructive technique for semiconductor characterization that relies on analyzing illumination-induced changes in the surface voltage. It is

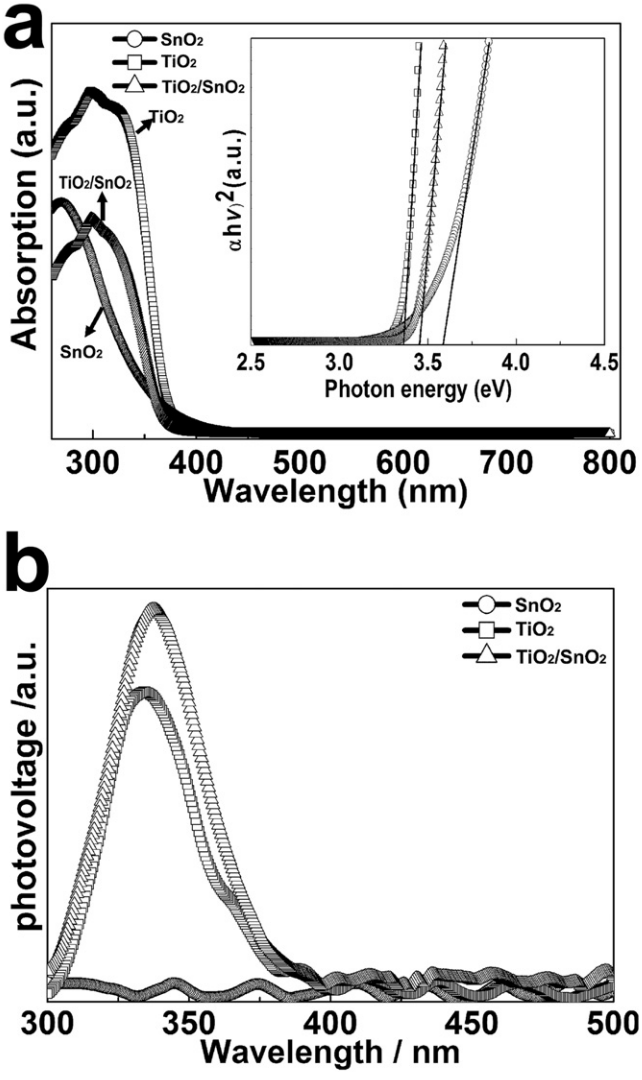

Fig. 3. (a) UV–vis absorption spectrum of TiO_2/SnO_2, SnO_2, and TiO_2 hollow spheres; the inset is the corresponding plot of $(h\nu)^2$ versus photon energy. (b) SPS of the TiO_2/SnO_2, SnO_2, and TiO_2 hollow spheres.

an effective tool for the investigation of the photoinduced charge-transfer properties in TiO_2/SnO_2 hollow spheres and may provide useful information for understanding the catalytic mechanism of the sample. From Fig. 3b, it can be seen that an apparent SPV response ranging from 300 to 390 nm is observed for TiO_2/SnO_2 and TiO_2 hollow spheres, whereas a quite weak SPV response is observed for SnO_2 hollow spheres. Compared with the TiO_2 hollow spheres, TiO_2/SnO_2 hollow spheres show a distinctly stronger SPV response, indicating that the photogenerated charges are more effectively separated for the latter material.

RhB, a chemically stable and poorly biodegradable dye contaminant in wastewater, is used to evaluate the photocatalytic ability of the TiO_2/SnO_2 hollow spheres. Fig. 4a shows the temporal absorption spectral changes of RhB in photo-degradation over the TiO_2/SnO_2 hollow sphere catalysts under UV-light irradiation. The result indicated that the absorption peak at 554 nm disappeared after irradiation for 15 min. The photocatalytic activity of TiO_2/SnO_2 hollow spheres is plotted in Fig. 4b, evaluated by the degradation examination of RhB solution under UV-light illumination. For comparison, the photocatalytic experiments were further carried out with the SnO_2 and TiO_2 hollow spheres. After 15 min illumination, the degradation of RhB in a direct photolysis process without any photocatalyst is negligible. The degradation efficiency of RhB by a photocatalytic process was 100% when TiO_2/SnO_2 hollow spheres existed. 80% and 9% of RhB were photocatalytic degraded when using TiO_2 and SnO_2 hollow spheres, respectively, under the same conditions. It is obvious that the TiO_2/SnO_2 hollow spheres exhibited a much higher photocatalytic activity. The stability of the TiO_2/SnO_2 heterojunction photocatalyst was also demonstrated by the recycling test (Fig. 4c). After four cycles of photocatalytic degradation, no significant loss of activity was represented. Based on the above photocatalytic results, it is demonstrated that the improved photocatalytic ability of the TiO_2/SnO_2 heterojunction photocatalyst could be attributed to the enhanced quantum yield promoted by the heterojunction, which was consistent with the observation in the SPV measurements. Additionally, the composite hollow spheres with high surface areas were in favor of the transfer of electrons and holes generated inside the crystal to the surface, and facilitated the degradation of RhB.

The charge separation mechanism of TiO_2/SnO_2 hollow spheres is shown in Fig. 4d. The whole process consists of the formation of charge carriers, the dissociation of charge carriers into free carriers, the transfer of free carriers to the surface, and the generation of active oxygen species such as •OH or $•O_2^-$. Under UV luminescence, the photogenerated carriers of electrons and holes appear in the conduction band (CB) and valence band (VB) for each semiconductor, respectively. As we know, the CB edges of SnO_2 and anatase TiO_2 are situated at $+0.07$ and -0.34 V versus normal hydrogen electrode (NHE) at pH 7, respectively. The VB edge of SnO_2 ($+3.66$ V) is more positive than that of anatase TiO_2 ($+3.02$ V) [8,24,25]. Under the potential driving force of TiO_2/SnO_2 heterojunction, the electrons (holes) transfer from the CB of TiO_2 (VB of SnO_2) to the CB of SnO_2 (VB of TiO_2). Due to the presence of a TiO_2/SnO_2 heterojunction, the probability of the recombination of electron-hole pairs is significantly reduced. Consequently, the highly efficient active oxygen species processes would occur for the degradation. It is proposed that the hole-related redox process plays a major role for the decomposition of RhB, because the CB potential of SnO_2 seems too low for the electron to reduce O_2 to generate $•O_2^-$ (the E < theta > ($O_2/•O_2^-$) is about -0.046 eV).

4. Conclusions

In conclusion, the TiO_2/SnO_2 hollow spheres have been fabricated by a facile two-step LPD method to attain excellent photocatalytic activities for the decomposition of RhB. The TiO_2/SnO_2 heterojunction structure can effectively promote an increase in the charge separation of the

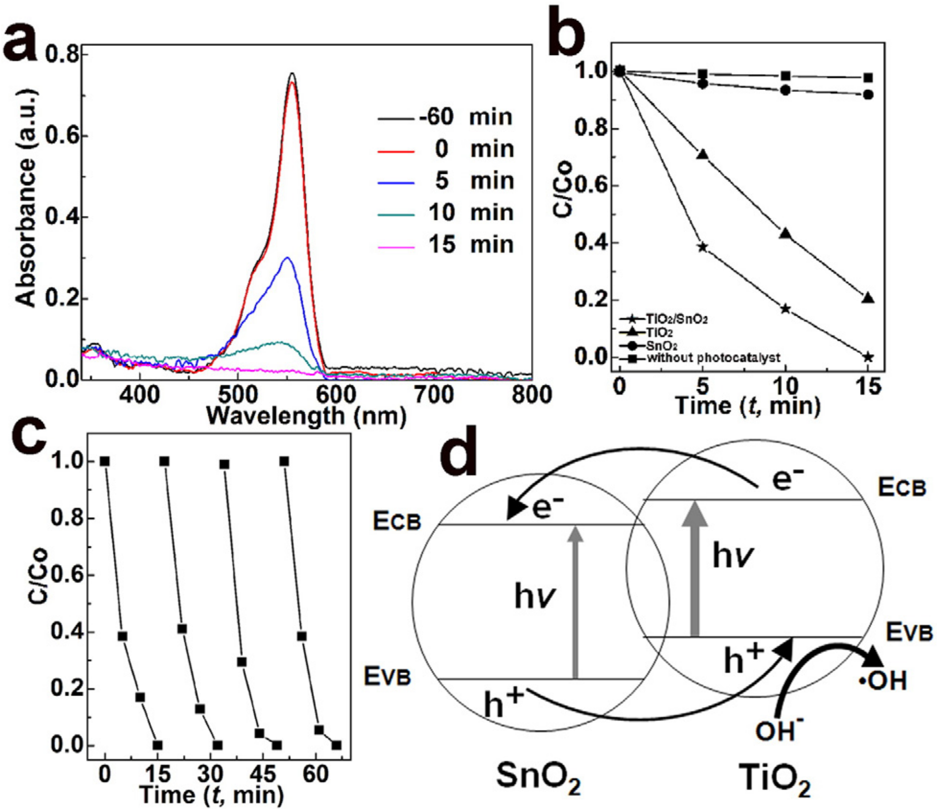

Fig. 4. (a) Time-dependent UV–vis absorption spectra of the RhB solution in the presence of TiO_2/SnO_2 hollow spheres. (b) Photocatalytic decomposition of RhB solution with TiO_2/SnO_2 hollow spheres, SnO_2 hollow spheres, TiO_2 hollow spheres, and without photocatalyst for reference. (c) Recyclability test of photocatalytic decomposition for TiO_2/SnO_2 hollow spheres. (d) Schematic band diagram of TiO_2/SnO_2 hollow spheres at thermal equilibrium and the transfer processes of photogenerated carriers (e^-, electrons; h^+, holes).

photogenerated electrons and holes within the composite structures to enhance photocatalytic reaction with respect to the performance of pure SnO_2 and TiO_2 hollow spheres. Furthermore, TiO_2/SnO_2 hollow sphere heterojunction shows no significant loss of activity in the recycling experiments. Considering the unique excellent properties of TiO_2 and SnO_2, the TiO_2/SnO_2 hollow spheres described herein presents a new approach which is expected to lead to a wide range of applications including photocatalysis, lithium ion batteries, and sensors.

Acknowledgments

This work was financially supported by the National Natural Science Foundation of China (NSFC) with no. 11364002, 51072066 and 51302040 and the Natural Science Foundation of Jiangxi with no. 20132BAB212004 and no. 20122BAB202011.

Appendix A. Supplementary data

Supplementary data to this article can be found online at http://dx.doi.org/10.1016/j.catcom.2014.11.032.

References

[1] K. Byrappa, A.K. Subramani, S. Ananda, K.M. LokanathaRai, R. Dinesh, M. Yoshimura, Bull. Mater. Sci. 29 (2006) 433–438.
[2] Y.T. Han, X. Wu, Y.L. Ma, L.H. Gong, F.Y. Qu, H.J. Fan, CrystEngComm 13 (2011) 3506–3510.
[3] W. Smith, W. Ingram, Y.P. Zhao, Chem. Phys. Lett. 479 (2009) 270–273.
[4] Y.F. Guo, X. Quan, N. Lu, H.M. Zhao, S. Chen, Environ. Sci. Technol. 41 (2007) 4422–4427.
[5] M.R. Hoffmann, S.T. Martin, W.Y. Choi, D.W. Bahnemann, Chem. Rev. 95 (1995) 69–96.
[6] K. Tennakone, J. Bandara, Appl. Catal. A 208 (2001) 335–341.
[7] W.W. Wang, Y.J. Zhu, L.X. Yang, Adv. Funct. Mater. 17 (2007) 59–64.
[8] M.H. Zhou, J.G. Yu, S.W. Liu, P.C. Zhai, L. Jiang, J. Hazard. Mater. 154 (2008) 1141–1148.
[9] P. Basyach, P. Chetri, A. Choudhury, Int. J. Sci. Eng. Res. 4 (2013) 28–31.
[10] I. Parmasivam, Y.-C. Nah, C. Das, N.K. Shrestha, P. Schmuki, Chem. Eur. J. 16 (2010) 8993–8997.
[11] Y. Liu, C.S. Xie, H.Y. Li, H. Chen, T. Zou, D.W. Zeng, J. Hazard. Mater. 196 (2011) 52–58.
[12] S.J. Ding, J.S. Chen, D.Y. Luan, F.Y.C. Boey, S. Madhavi, X.W. Lou, Chem. Commun. 47 (2011) 5780–5782.
[13] X.W. Lou, Y. Wang, C.L. Yuan, J.Y. Lee, L.A. Archer, Adv. Mater. 18 (2006) 2325–2329.
[14] K.K. Akurati, A. Vital, R. Hany, B. Bommer, T. Graule, M. Winterer, Int. J. Photogr. 7 (2005) 153–161.
[15] Z.Y. Liu, D.L. Darren, P. Guo, J.O. Leckie, Nano Lett. 7 (2007) 1081–1085.
[16] S.H. Hwand, C. Kim, J. Jang, Catal. Commun. 12 (2011) 1037–1041.
[17] S.N. Chai, G.H. Zhao, P.Q. Li, Y.Z. Lei, Y.N. Zhang, D.M. Li, J. Phys. Chem. C 115 (2011) 18261–18269.
[18] J. Yu, X.X. Yu, B.B. Huang, X.Y. Zhang, Y. Dai, Cryst. Growth Des. 9 (2009) 1474–1480.
[19] T.Z. Tong, J.L. Zhang, B.Z. Tian, F. Chen, D.N. He, Mater. Lett. 62 (2008) 2970–2972.
[20] J. Yi, X.P. Li, S.J. Hu, W.S. Li, R.H. Zeng, Z. Fu, L. Chen, Rare Metals 30 (2011) 589–594.
[21] Y. Matsushima, R. Satoh, T. Kawai, K. Maeda, T. Suzuki, J. Ceram. Soc. Jpn. 118 (2010) 206–212.
[22] Y. Masuda, N. Saito, R. Hoffmann, M.R. De Huire, K. Koumoto, Sci. Technol. Adv. Mater. 4 (2003) 461–467.
[23] H. Strohm, P. Lobmamnn, Chem. Mater. 17 (2005) 6772–6780.
[24] A. Hattori, Y. Tokihisa, H. Tada, S. Ito, J. Electrochem. Soc. 147 (2000) 2279–2283.
[25] J. Shang, W. Yao, Y. Zhu, N. Wu, Appl. Catal. A 257 (2004) 25–32.